



# On Using Inspiring Supermassive Binary Black Holes in the PTA Frequency Band as Standard Sirens to Constrain Dark Energy

Changshuo Yan<sup>1,2</sup>, Wen Zhao<sup>3,4</sup>, and Youjun Lu<sup>1,2</sup><sup>1</sup> CAS Key Laboratory for Computational Astrophysics, National Astronomical Observatories, Chinese Academy of Sciences, Beijing, 100101, People's Republic of China; [yancs@nao.cas.cn](mailto:yancs@nao.cas.cn), [luyj@nao.cas.cn](mailto:luyj@nao.cas.cn)<sup>2</sup> School of Astronomy and Space Science University of Chinese Academy of Sciences, Beijing, 100049, People's Republic of China<sup>3</sup> CAS Key Laboratory for Researches in Galaxies and Cosmology, Department of Astronomy, University of Science and Technology of China, Chinese Academy of Sciences, Hefei, Anhui 230026, People's Republic of China; [wzhao7@ustc.edu.cn](mailto:wzhao7@ustc.edu.cn)<sup>4</sup> School of Astronomy and Space Science, University of Science and Technology of China, Hefei, 230026, People's Republic of China

Received 2019 October 29; revised 2019 December 5; accepted 2019 December 9; published 2020 January 28

## Abstract

Supermassive binary black holes (SMBBHs) in galactic centers may radiate gravitational waves (GW) in the nano-Hertz frequency band, which are expected to be detected by pulsar timing arrays (PTAs) in the near future. GW signals from individual SMBBHs at cosmic distances, if detected by PTAs, are potentially powerful standard sirens that can be used to independently measure distances and thus put constraints on cosmological parameters. In this paper, we investigate the constraint that may be obtained on the equation of state ( $w$ ) of dark energy by using those SMBBHs, expected to be detected by the PTAs in the Square Kilometre Array (SKA) era. By considering both the currently available SMBBH candidates and mock SMBBHs in the universe resulting from a simple galaxy major merger model, we find that  $\sim 200$ – $3000$  SMBBHs with chirp mass  $> 10^9 M_\odot$  are expected to be detected with a signal-to-noise ratio  $> 10$  by SKA–PTA with conservative and optimistic settings and they can be used to put a constraint on  $w$  to an uncertainty of  $\Delta w \sim 0.02$ – $0.1$ . If further information on the mass and mass ratio of those SMBBHs can be provided by electromagnetic observations (e.g., chirp mass uncertainty  $\lesssim 50\%$ ), the constraint may be further improved to a  $\lesssim 0.01$  level, as many more SMBBHs will be detected by SKA–PTA with relatively better distance measurements and can be used as the standard sirens.

*Unified Astronomy Thesaurus concepts:* Supermassive black holes (1663); Gravitational waves (678); Gravitational wave astronomy (675); Dark energy (351); Cosmological parameters (339); Active galactic nuclei (16); Fisher's Information (1922); Black hole physics (159); Pulsar timing method (1305)

## 1. Introduction

It is crucial to accurately measure the cosmological parameters for understanding the dynamical evolution of the universe and the nature of dark matter and dark energy. Numerous methods have been developed to achieve this goal. However, current available measurements obtained by using different methods may have significant discrepancy, e.g., the  $4.4\sigma$  discrepancy between the Hubble constant ( $H_0$ ) inferred from the Planck cosmic microwave background (CMB) data and that obtained from SN Ia standard candles (see Planck Collaboration et al. 2018; Riess et al. 2019). This “Hubble tension” may be an indicator of new physics beyond the standard Lambda cold dark matter ( $\Lambda$ CDM) cosmology or unknown systemic biases in those current methods. Therefore, it is important to propose and apply other (new) method(s) to independently measure cosmological parameters and compare them with those traditional methods for improving the measurement accuracy of the cosmological parameters.

Gravitational wave (GW) from a compact binary coalescence (CBC) provides a new type of “standard siren” to independently probe cosmological parameters, if its redshift can be measured (Schutz 1986; Chernoff & Finn 1993; Finn 1996). The first multimessenger detection of a double neutron star (DNS) merger, GW170817 (Abbott et al. 2017a, 2017b), has enabled the first standard siren measurement of  $H_0$  (Abbott et al. 2017c; Hotokezaka et al. 2019), and demonstrated the great potential of this unbiased method (e.g., Zhao et al. 2011; Chen et al. 2018; Zhao & Wen 2018). However, only mergers of DNSs and black hole–neutron star binaries are expected to

have significant electromagnetic (EM) signals (though weak), with which their redshift information can be obtained. Large fraction of the sources detected by ground-based GW detectors would be mergers of stellar-mass binary black holes (sBBHs), which may not be accompanied with significantly bright EM counterparts as current searches for their EM counterparts all returned a null result (e.g., Noysena et al. 2019). This may significantly limit the distance and number of GW sources that can be used as the standard sirens, and thus limit the power of this method to measure the cosmological parameters and constrain the nature of dark matter and dark energy.

Inspiring of a supermassive binary black hole (SMBBHs; with mass  $\gtrsim 10^8 M_\odot$ ) in galactic centers is important GW sources at  $10^{-9}$ – $10^{-6}$  Hz, which are long anticipated to be detected by pulsar timing arrays (PTAs; Rajagopal & Romani 1995; Jaffe & Backer 2003; Wyithe & Loeb 2003; Sesana 2013; Ravi et al. 2014; Perera et al. 2018). Most traditional PTA studies focus on the detection of the stochastic GW background from numerous cosmic SMBBHs (e.g., Jenet et al. 2006; Lentati & Shannon 2015; Shannon et al. 2015; Arzoumanian et al. 2016, 2018a, 2018b; Desvignes et al. 2016; Reardon et al. 2016; Sesana et al. 2018; Perera et al. 2019), while recent PTA studies begin to investigate the detectability of individual SMBBHs\*\*\* (Sesana et al. 2009; Corbin & Cornish 2010; Finn & Lommen 2010; Sesana & Vecchio 2010; Lee et al. 2011; Babak & Sesana 2012; Ellis et al. 2012; Ravi et al. 2014; Wang et al. 2014; Arzoumanian et al. 2014; Zhu et al. 2015; Madison et al. 2016; Wang & Mohanty 2017; Aggarwal et al. 2019) and find that the loudest SMBBHs may

have rather high signal-to-noise ratios (S/Ns) to be detected by future PTAs, such as the Square Kilometre Array (SKA) PTA (e.g., Ravi et al. 2015; Rosado et al. 2015).

It is possible that future ‘‘PTA detected SMBBHs’’ can also be taken as the standard sirens to probe cosmology. Different from sBBHs, many SMBBHs may have EM counterparts and thus can be detected by EM waves with redshift measurements. Simulations have also shown that the physical parameters of SMBBH systems (including the luminosity distance) detected by future PTA(s) can be extracted with high accuracy (e.g., Wang et al. 2014; Zhu et al. 2015; Wang & Mohanty 2017). Therefore, conceptually it is undoubtable that those PTA SMBBHs can be used as standard sirens. However, whether these ‘‘PTAs detected SMBBHs’’ can provide sufficiently interesting measurements on the cosmological parameters depends on their foreseeable S/Ns and number distribution as a function of redshift. In this paper, we will investigate the potential of using future ‘‘PTA detected SMBBHs’’ as standard sirens to probe cosmological parameters, especially on constraining the nature of dark energy.

This paper is organized as follows. In Section 2, we introduce a method of using Fisher information matrix to analyze the GW signal from SMBBHs and determine measurement errors of various physical parameters involved in. We show how to obtain constraints on the dark energy by using PTAs SMBBHs in Section 3. We illustrate the effects of different physical parameters of the GW sources on the GW detection and the errors of luminosity distance measurements in Section 4. In Sections 5, we apply the above method to the currently available SMBBH candidates from astronomical observations and the mock SMBBH samples obtained from a simple model, respectively, and predict the robustness of the constraints that can be obtained from PTA SMBBHs. Conclusions and discussions are given in Section 6.

Throughout the paper, we adopt a flat  $\Lambda$ CDM cosmology with  $\Omega_m = 0.3$ ,  $\Omega_\Lambda = 0.7$ ,  $h = 0.7$ , where  $h = H_0/100 \text{ km s}^{-1} \text{ Mpc}^{-1}$  (e.g., see Planck Collaboration et al. 2016).

## 2. GW Signal and Analysis Method

A PTA data set is the time of arrivals (ToAs) for pulses from millisecond stable pulsars (MSPs) monitored over a decade or longer with typical cadence of biweekly to monthly (Desvignes et al. 2016; Reardon et al. 2016; Arzoumanian et al. 2018b; Perera et al. 2019). The ToA data encodes the information of the MSPs’ rotation, the dispersion due to the ionized interstellar medium, and also the binary behavior of the MSP if it is in a binary system, which can be well revealed by standard models. The GW effects can be seen in the ToA residuals by removing the model-predicted TOAs from the observational TOA data, and various noise processes can be constrained and included in the timing model (Lentati et al. 2016). The root mean square (rms) of these time residuals reflects the stability of the pulsar and the quality of the timing data that can be used to measure or constrain the GW signal(s).

Consider a single GW source coming from a direction  $\hat{\Omega}$ , its induced pulsar timing residuals measured at time  $t$  on the Earth can be written as (e.g., see Zhu et al. 2015)

$$s(t, \hat{\Omega}) = F^+(\hat{\Omega})\Delta A_+(t) + F^\times(\hat{\Omega})\Delta A_\times(t), \quad (1)$$

where  $F^+(\hat{\Omega})$  and  $F^\times(\hat{\Omega})$  are the antenna pattern functions as given by (Wahlquist 1987):

$$\begin{aligned} F^+(\hat{\Omega}) &= \frac{1}{4(1 - \cos\theta)} \{ (1 + \sin^2\delta)\cos^2\delta_p \cos[2(\alpha - \alpha_p)] \\ &\quad - \sin 2\delta \sin 2\delta_p \cos(\alpha - \alpha_p) + \cos^2\delta(2 - 3\cos^2\delta_p) \}, \\ F^\times(\hat{\Omega}) &= \frac{1}{2(1 - \cos\theta)} \{ \cos\delta \sin 2\delta_p \sin(\alpha - \alpha_p) \\ &\quad - \sin\delta \cos^2\delta_p \sin[2(\alpha - \alpha_p)] \}. \end{aligned} \quad (2)$$

Here  $(\alpha, \delta)$  or  $(\alpha_p, \delta_p)$  are the R.A. and decl. of the GW source or pulsar, and  $\theta$  is the opening angle between the GW source and pulsar with respect to the observer

$$\cos\theta = \cos\delta \cos\delta_p \cos(\alpha - \alpha_p) + \sin\delta \sin\delta_p. \quad (3)$$

In Equation (1),  $\Delta A_{\{+, \times\}}(t) = A_{\{+, \times\}}(t) - A_{\{+, \times\}}(t_p)$ , where  $t_p = t - d_p(1 - \cos\theta)/c$  is the time at which the GW passes the MSP with  $d_p$  representing the pulsar distance, and  $A_{\{+, \times\}}(t)$  and  $A_{\{+, \times\}}(t_p)$  contribute to the Earth term and pulsar term, respectively, for which the specific functional forms depend on the type of sources being searched for. For cases considered in the present paper, we assume evolving SMBBHs and thus the frequency of the Earth term and pulsar term are not exactly the same, though the difference is tiny for most cases. For SMBBHs on circular orbits, we have

$$\begin{aligned} A_+(t) &= \frac{h_0(t)}{2\pi f(t)} \{ (1 + \cos^2\iota)\cos 2\psi \sin[\phi(t) \\ &\quad + \phi_0] + 2\cos\iota \sin 2\psi \cos[\phi(t) + \phi_0] \}, \end{aligned} \quad (4)$$

$$\begin{aligned} A_\times(t) &= \frac{h_0(t)}{2\pi f(t)} \{ (1 + \cos^2\iota)\sin 2\psi \sin[\phi(t) \\ &\quad + \phi_0] - 2\cos\iota \cos 2\psi \cos[\phi(t) + \phi_0] \}. \end{aligned} \quad (5)$$

Here  $\iota$  is the angle between the normal of the binary orbital plane and the line of sight,  $\psi$  is the GW polarization angle,  $\phi_0$  is a phase constant, and  $h_0$  is the intrinsic GW strain amplitude defined as

$$h_0 = 2 \frac{(GM_c^z)^{5/3} (\pi f)^{2/3}}{c^4 d_L} = 2 \frac{(GM_c)^{5/3} (\pi f_r)^{2/3}}{c^4 d_c}, \quad (6)$$

with  $d_L$  and  $d_c$  representing the luminosity and comoving distance to the source, respectively,  $M_c = M_{*,1}^{3/5} M_{*,2}^{3/5} (M_{*,1} + M_{*,2})^{-1/5}$  representing the binary chirp mass,  $M_{*,1}$  and  $M_{*,2}$  ( $\leq M_{*,1}$ ) representing the SMBBH component masses. Noted here that only the redshifted chirp mass  $M_c^z = M_c(1+z)$ , but not the chirp mass, is directly measurable from GW data; likewise, the rest-frame frequency  $f_r$  is related to the observed frequency  $f$  by  $f = f_r/(1+z)$  (Maggiore 2008). This is the reason that independent measurements of the redshifts of GW sources are required for GW cosmology studies, in order to break such a degeneracy between GW measured mass and redshift.

In the quadrupole approximation, the GW phase and frequency that appear in Equations (4) and (5) are given by

$$f(t) = \left[ f_0^{-8/3} - \frac{256}{5} \pi^{8/3} \left( \frac{GM_c^z}{c^3} \right)^{5/3} t \right]^{-3/8}, \quad (7)$$

$$\phi(t) = \frac{1}{16} \left( \frac{GM_c^z}{c^3} \right)^{-5/3} \{ (\pi f_0)^{-5/3} - [\pi f(t)]^{-5/3} \}, \quad (8)$$

where  $f_0$  is the observed GW frequency at the time of the first observation (e.g., Thorne 1987).

We define the S/N of the GW signal detected by PTAs with  $N_p$  MSPs as

$$\rho^2 = \sum_{j=1}^{N_p} \sum_{i=1}^N \left[ \frac{s_j(t_i)}{\sigma_{t,j}} \right]^2, \quad (9)$$

where  $N$  is the total number of data points for each MSP,  $s_j(t_i)$  is the timing residuals of  $j$ th MSP at time  $t_i$  (see Equation (1)), and  $\sigma_{t,j}$  is the rms of timing noises of the  $j$ th MSP. In this paper, we adopt the Fisher information matrix for parameter estimations. In the case of a network including  $N_p$  independent MSPs, the Fisher matrix is

$$\Gamma_{ab} = \sum_{j=1}^{N_p} \sum_{i=1}^N \frac{\partial s(t_i)}{\sigma_{t,j} \partial p_a} \frac{\partial s(t_i)}{\sigma_{t,j} \partial p_b}, \quad (10)$$

where  $p_a$  and  $p_b$  denote the free parameters to be estimated.

For each given GW source, the response of the pulsar network depends on  $N_p + 8$  system parameters, including those of the GW source (i.e.,  $M_c$ ,  $\alpha$ ,  $\delta$ ,  $\iota$ ,  $\psi$ ,  $\phi_0$ ,  $f_0$ ,  $d_L$ ) and distances of MSPs  $d_{p,j}$  ( $j = 1, 2, \dots, N_p$ ). Prior information can be included as  $\Gamma_{ab} \rightarrow \Gamma_{ab} - \left\langle \frac{\partial^2 \ln P(p_i)}{\partial p_a \partial p_b} \right\rangle$ , where  $P(p_i)$  is the prior distribution of the parameter  $p_i$  (e.g., see Albrecht et al. 2009). For the inclination angle  $\iota$  we need to consider its prior distribution. As the disk direction is randomly distribute in the  $4\pi$  solid angle, so the  $P(\iota) \propto \sin(\iota)$ , then we will have  $\Gamma_{ii} \rightarrow \Gamma_{ii} + \frac{1}{\sin^2 \iota}$  where  $p_i = \iota$ . If the GW sources can be identified electromagnetically, then the sky location, redshift, and even the SMBBH mass can be obtained, which may add some additional information into the Fisher matrix. In this case, a Gaussian prior with width  $\sigma_i$  may be placed on the  $i$ th parameter, with additional EM information, by adding to the appropriate diagonal element of the Fisher matrix:  $\Gamma_{ab} \rightarrow \Gamma_{ab} + \delta_{ai} \delta_{bi} / \sigma_i^2$ . The Fisher matrix is commonly used in many fields to estimate errors in the measured parameters by the expression  $\langle \delta p_a \delta p_b \rangle = (\Gamma^{-1})_{ab}$ . Once the Fisher matrix  $\Gamma_{ab}$  is calculated, the error in measuring the parameter  $p_a$  can then be estimated as  $\Delta p_a = (\Gamma^{-1})_{aa}^{1/2}$ .

### 3. Constraining Dark Energy

In a flat universe, the luminosity distance can be written as

$$d_L = (1+z) \int_0^z \frac{dz'}{H(z')}, \quad (11)$$

where  $H(z)$  is the Hubble parameter. Given a form of dark energy with density parameter  $\Omega_{de}$  and a (constant) equation-of-state (EoS) index  $w$ , one has

$$H(z) = H_0 [\Omega_m (1+z)^3 + \Omega_{de} (1+z)^{3(1+w)}]^{1/2}. \quad (12)$$

Similar to Arun et al. (2009), we are interested in getting a rough sense of the level of accuracy we can expect in extracting the EoS index of dark energy  $w$ . From the expression of  $d_L$ , it seems possible that one can constrain the full parameter set  $(H_0, \Omega_m, \Omega_{de}, w)$  together by the GW data alone, as long as the redshifts of GW sources are known. Unfortunately, in the

previous work (Zhao et al. 2011), we found that these globe constraints cannot be realized, due to the strong degeneracy between the background parameters  $(H_0, \Omega_m, \Omega_{de})$  and the dark energy EoS  $w$ . The same problem also happens in other methods for dark energy detection (e.g., SN Ia and BAO methods). A general way to break this degeneracy is to combine the result with the CMB data, which are sensitive to the background parameters  $(H_0, \Omega_m, \Omega_{de})$ , and provide the necessary complement to the GW data. It has also been discovered in Zhao et al. (2011) that taking the CMB observation as a prior is nearly equivalent to treating the parameters  $(H_0, \Omega_m, \Omega_{de})$  as known in the data analysis. Thus, we use the GW data to constrain the parameters  $w$  only. For a single GW source, the error on  $w$  can be estimated as

$$\Delta w = d_L \left| \frac{\partial d_L}{\partial w} \right|^{-1} \frac{\sigma_{d_L}}{d_L}. \quad (13)$$

Note that the uncertainty  $\sigma_{d_L} = \sqrt{(\Delta d_L)^2 + (\tilde{\Delta} d_L)^2}$ , where  $\Delta d_L$  is calculated by the Fisher matrix analysis as above, and

$$\tilde{\Delta} d_L = d_L \times 0.066 \left( \frac{1 - (1+z)^{-0.25}}{0.25} \right)^{1.8}, \quad (14)$$

which accounts for the uncertainty caused by weak lensing (Hirata et al. 2010).

If we consider a set of GW sources, and  $\Delta w_i$  denotes the result of  $\Delta w$  derived from the  $i$ th GW source. Then the combined constraint becomes

$$\Delta w = \frac{1.0}{\sqrt{\sum_i (\Delta w_i)^{-2}}}. \quad (15)$$

### 4. Effects of Physical Parameters of the GW Sources

To figure out the effects of the physical parameters of an SMBBH on the GW detection S/N and the distance measurement, we construct an SKA era PTA by using the simulated pulsar catalog in Smits et al. (2009). In principle, the choice of MSPs depends on their potential timing accuracy, which mainly depends on the stability of the rotation of MSP itself, and the accuracy of TOA we detect. The neighboring MSPs may have a higher flux, and the integrated pulse profile has a higher S/N and a more accurate timing. In addition, the impact of dispersion and other effects is small. For these reasons, similar to Wang & Mohanty (2017), in this paper we select 1026 MSPs within 3 kpc from the Earth for the analysis. Figure 1 shows the localization of those simulated MSPs. With this assumed SKA-PTA, we generate the data realizations by adopting a uniform cadence, for simplicity, either 1 week or 2 weeks, while the typical cadence of current PTAs are biweekly to monthly. The span of the simulated timing residuals is 10 yr. Rms of timing noises are assumed to be 20 ns, 50 ns, and 100 ns for each MSP, respectively, here we assumed three different values for each simulated pulsar to investigate how the timing precision of pulsars affects the results.

We will first investigate some SMBBH candidates with typical period  $\sim 1-10$  yr that are available in the literature, as the main GW sources in the PTAs frequency band are SMBBHs. Taking one of them, SDSS J164452.71+430752.2, at redshift  $z = 1.715$ , as an example, we investigate the effects of inclination angle  $\iota$  and mass ratio  $q$

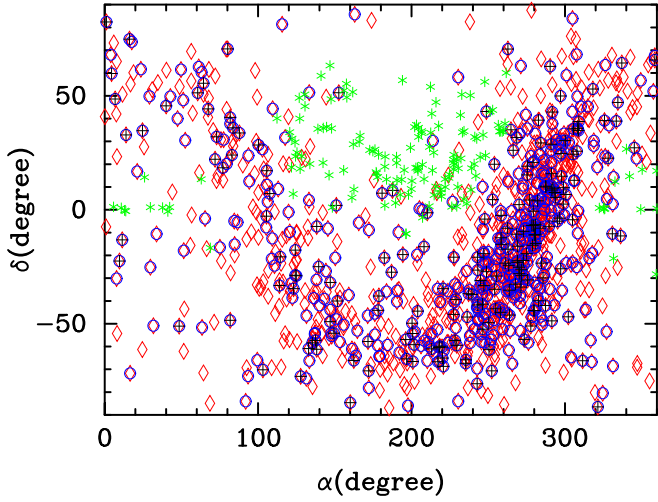
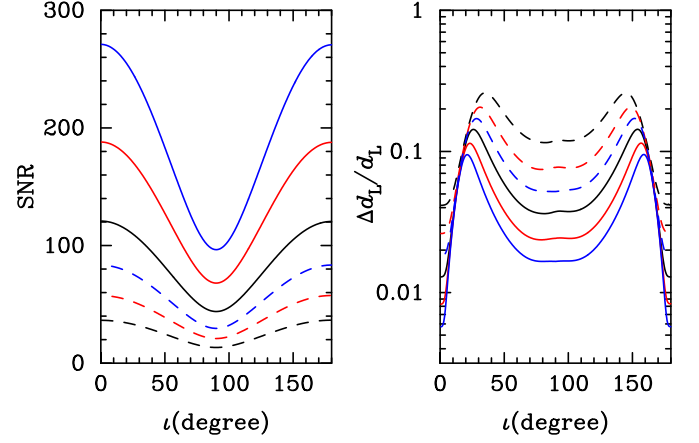


**Figure 1.** Positions of the selected 1026 MSPs constituting the simulated SKA-PTA and current available SMBBH candidates on the sky. Red diamonds show all of those 1026 MSPs, while blue circles and black pluses (+) show 500 and 200 out of them, respectively. These three different MSP samples are all used in the paper. Green stars show the SMBBH candidates obtained from observations.

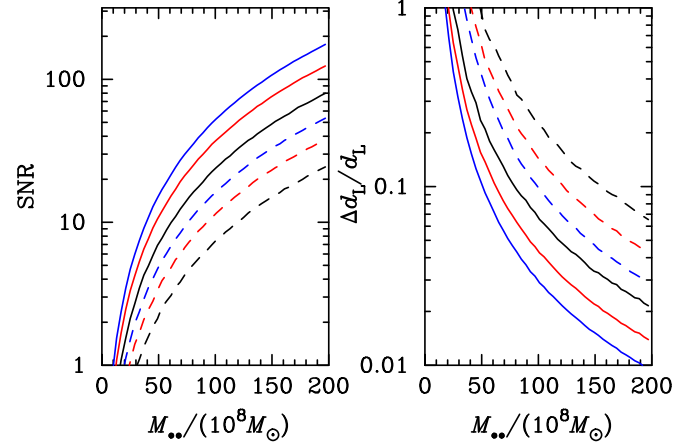
on the S/N of its GW signal (see Equation (9)) and relative error of luminosity distance  $\Delta d_L/d_L$ . The total mass of this SMBBH is estimated to be  $M_{**} \sim 1.41 \times 10^{10} M_\odot$  (Shen et al. 2008), and the GW radiation from it is almost monochromatic with a frequency of  $f_0 \simeq 1.16 \times 10^{-8}$  Hz if it is on a circular orbit. Note that in the calculation of  $\Delta d_L/d_L$ , we adopt the Fisher matrix analysis, for which  $\alpha$  and  $\delta$  are fixed as it was accurately determined by its EM counterparts, but not excluded in the analysis if not otherwise stated, and we also further consider the case if the information about the total mass and mass ratio of SMBBH can be given by EM observations. In our calculations, we consider the cases with different numbers of MSPs, i.e.,  $N_p = 1026$ ,  $N_p = 500$ , and  $N_p = 200$ , respectively. Our main results are plotted in Figures 2–4, respectively.

Figure 2 shows the resulting S/N and relative error of luminosity distance  $\Delta d_L/d_L$  as a function of  $\iota$ . As seen from this figure, a larger  $q$  for a system with given total mass, correspondingly a larger  $M_c$ , results in a larger S/N and a smaller  $\Delta d_L/d_L$ . If  $\iota = 0$ , i.e., the GW source is face-on, the resulting S/N is then the largest and the GW signal can be more easily detected, the resulting  $\Delta d_L/d_L$  show that the luminosity distance can be well determined for a face-on or edge-on source and this value will peak at an angle in a range of  $\iota \in (20^\circ, 50^\circ)$  or  $(130^\circ, 160^\circ)$ . These results are consistent with the results for the ground-based GW detectors (e.g., Abbott et al. 2019).

Figures 3 and 4 show the dependence of the resulting S/N and  $\Delta d_L/d_L$  on the total mass and GW frequency of the system with fixed  $\iota = \pi/2$ , respectively. As seen from these Figures, the larger the total mass of the system, the larger the resulting S/N and the smaller the resulting  $\Delta d_L/d_L$ ; the larger the initial GW frequency  $f_0$ , the smaller the resulting S/N and the smaller the resulting  $\Delta d_L/d_L$ , except at  $f_0 \gtrsim 4 \times 10^{-8}$  Hz. The larger  $f_0$  means the smaller semimajor axis of the SMBBH system and the larger change rate of the frequency, which leads to a better determination of the luminosity distance  $d_L$ , but a decrease of S/N as it  $\propto f^{-1/3}$ . The rapid decrease of S/N at  $f_0 \gtrsim 4 \times 10^{-8}$  Hz is due to those SMBBH systems having a merger timescale  $\tau_{\text{GW}}$  less than the observation period (e.g.,  $T_{\text{obs}} = 10$



**Figure 2.** Dependence of the resulting S/N (left panel) and relative error of luminosity distance (right panel) on  $\iota$ , obtained for the SMBBH candidate SDSS J164452.71+430752.2 with  $M_{**} = 1.413 \times 10^{10} M_\odot$  and  $f_0 = 1.16 \times 10^{-8}$  Hz. In each panel, the blue, red, and black solid lines show the results for the cases with  $(N_p, q) = (1026, 1)$ ,  $(500, 1)$ , and  $(200, 1)$ , respectively, while blue, red, and black dashed lines show the results for the cases with  $(N_p, q) = (1026, 0.1)$ ,  $(500, 0.1)$ , and  $(200, 0.1)$ , respectively. The assumed “PTA” here monitors 1026 pulsars with a cadence of 2 weeks and timing noise rms of 100 ns.



**Figure 3.** Dependence of the resulting S/N and  $\Delta d_L/d_L$  on the total mass of the system  $M_{**}$  with  $f_0 = 1.157 \times 10^{-8}$  Hz and  $\iota = \pi/2$ . Legend for the lines is similar to that in Figure 2. The assumed “PTA” here monitors 1026 pulsars with a cadence of 2 weeks and timing noise rms of 100 ns.

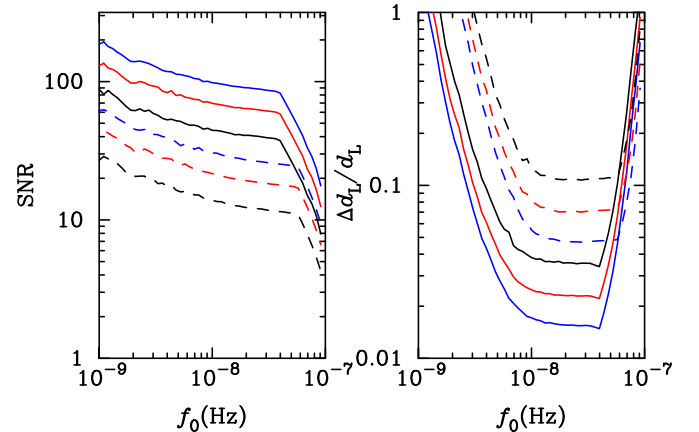


**Figure 4.** Dependence of the resulting S/N and  $\Delta d_L/d_L$  on the GW frequency of the system with  $M_{**} = 1.413 \times 10^{10} M_\odot$  and  $\iota = \pi/2$ . Legend for the lines is similar to that in Figure 2. The assumed “PTA” here monitors 1026 pulsars with a cadence of 2 weeks and timing noise rms of 100 ns.

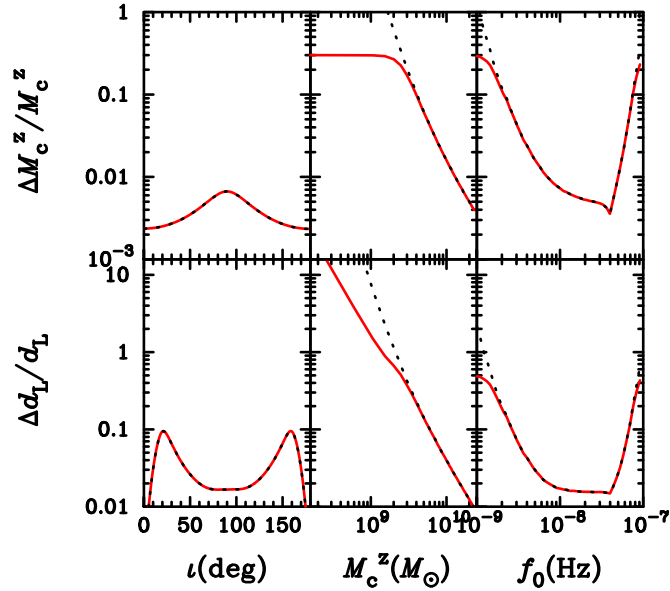


**Figure 5.** Dependence of the resulting  $\Delta M_c^z / M_c^z$  and  $\Delta d_L / d_L$  on inclination angle (left panel), redshifted chirp mass  $M_c^z$  (middle panel) and frequency  $f_0$  (right panel) expected from the “PTA observations” of sets of SMBBH systems with redshift  $z = 1.715$  and mass ratio  $q = 1$ . In each panel, the black dotted line shows the result obtained by considering all eight parameters of the GW source as free ones in the Fisher Matrix, while the red solid line shows the case by adding additional information on the redshifted chirp mass, following a Gaussian distribution with a scatter of  $\sigma \ln M_c^z = 0.3$  in the Fisher Matrix. The assumed “PTA” here monitors 1026 pulsars with a cadence of 2 weeks and timing noise rms of 100 ns.

yr) and thus  $S/N \propto \tau_{\text{GW}}^{1/2} \propto f^{-\gamma}$  with  $\gamma > 4/3$  as SMBBHs at this stage are not continuous GW sources and  $f$  increases quickly.

Additional information on the (total) mass and mass ratio of the PTA SMBBHs may be obtained from the EM measurements, and the degeneracy between chirp mass and frequency can thus be broken, leading to a significant improvement of the  $d_L$  estimation. Figure 5 shows the errors for luminosity distance estimates  $\Delta d_L$  from the PTA data only (black dotted lines in each panel) and those for the estimates from the PTA data with additional information on the redshifted chirp mass  $M_c^z$  (red solid line in each panel), respectively. In each panel, the black dotted lines show the results obtained by considering all eight parameters of the GW source as free ones in the Fisher Matrix, while the red solid line shows the cases by adding additional information on the redshifted chirp mass, following a Gaussian distribution with a scatter of  $\sigma \ln M_c^z = 0.3$  in the Fisher Matrix. Left panel shows  $\Delta d_L / d_L$  against the inclination angle  $\iota$  of the system. Middle panel shows that against the input total mass of the PTAs SMBBHs, and right panel shows  $\Delta d_L / d_L$  against the input  $f_0$  of the PTAs SMBBHs. According to this figure, if the errors of the redshifted chirp mass can be obtained from the EM observations, e.g., via the reverberation mapping method (independent of the cosmological model), with high precision, the measurement errors in  $d_L$  can be significantly suppressed, especially when  $f_0 \lesssim 10^{-8}$  Hz and  $M_{\bullet}$  in the range of  $\sim 10^9 - 10^{10} M_\odot$ . Since the number density of SMBBHs with  $M_{\bullet} \sim 10^9 M_\odot$  is much larger than that with  $M_{\bullet} \sim 10^{10} M_\odot$ , the number of PTA SMBBHs that can be used as standard sirens to constrain cosmology may increase significantly if additional information can be provided by electromagnetic observations and thus lead to better constraints on cosmology.

## 5. PTA SMBBHs as Standard Sirens

The detection of GWs from SMBBHs via PTAs has long been anticipated, but no GW from a single SMBBH has been detected in the past. Electromagnetic observations do suggest a number of SMBBH candidates but it is unclear how many of those SMBBH candidates are true SMBBHs. In this section, we will first consider those SMBBH candidates and then consider a mock sample of SMBBHs obtained from a simple galaxy merger model, in order to investigate possible constraints on the dark energy that may be obtained if assuming all those SMBBHs are true SMBBHs via future PTA observations.

One of the crucial points for using PTA SMBBHs to constrain cosmological parameters is to detect these systems by electromagnetic waves and get redshift measurements. Since SMBBHs are formed by mergers of galaxies, nuclear activities are believed to be triggered in many of such SMBBH systems with distinct signatures. For this reason, many SMBBH systems should be detectable via electromagnetic wave, which offers redshift measurement. Indeed, there have been a lot of efforts made in the past several decades to search for SMBBHs through their electromagnetic signatures, including the periodic variation in light curves (e.g., Valtonen et al. 2008; Graham et al. 2015a; Charisi et al. 2016), double-peaked or asymmetric broad emission lines (e.g., Liu et al. 2014; Li et al. 2016, 2019; Guo et al. 2019), UV-optical deficit in the spectral energy distribution (Yan et al. 2015; Zheng et al. 2016), etc. These efforts have resulted in more than 100 SMBBH candidates, though more efforts are still needed to confirm them. In the following calculations, therefore, we assume that the redshift of all PTA SMBBHs can be obtained by electromagnetic observations.<sup>5</sup> Note that we also ignore the effects due to dynamical environments of active SMBBHs on the orbital decay in addition to the GWs. This should also lead to some uncertainties in the use of PTA SMBBHs as standard sirens, but may be corrected by detailed studies of each individual source.

### 5.1. SMBBH Candidates from EM Observations

We adopt the current available sample for SMBBH candidates (154) obtained from various characteristic signatures with estimates on total masses  $M_{\bullet}$  and orbit period  $T$ . Among these SMBBH candidates, most (149) are obtained via periodic variations in their light curves (Graham et al. 2015a, 2015b; Charisi et al. 2016), others are Mrk 231 from Yan et al. (2015), NGC 5548 from Li et al. (2016), OJ 287 from Valtonen et al. (2008), SDSS J0159+0105 from Zheng et al. (2016), and Ark 120 from Li et al. (2019). The mass ratio  $q$ , inclination angle  $\iota$ , polarization angle  $\psi$ , and initial phase  $\phi_0$  of most SMBBH candidates are not known, yet. For this reason, we shall consider (1) two different mass ratios, i.e.,  $q = 1$  and 0.1, respectively, for those SMBBH candidates with no information on their mass ratios; (2) different  $\iota$  values. However, we fix  $\psi = 0$  and  $\phi_0 = 0$  as these two angles have no significant effects on the results. We also assume that those SMBBH candidates are all on circular orbits. Therefore, the orbit frequency  $f_{\text{orb}}$  is  $\frac{1}{2\pi} \sqrt{GM_{\bullet}/a^3}$ , where  $a$  is the orbital

<sup>5</sup> Note that some SMBBHs may be quiescent, which are indeed not easy to detect electromagnetically. Ignoring this should not affect our conclusion qualitatively.

**Table 1**

Expected Constraints on the Equation of State of Dark Energy from Current Available SMBBH Candidates

$\Delta t$ (week)	$\sigma_t$ (ns)	$N_p$	$\sigma \ln M_c^z$	$q = 1$		$q = 0.1$	
				$N_s$	$\Delta w$	$N_s$	$\Delta w$
2	100	200	...	11	0.17	2	0.63
2	100	500	...	14	0.12	2	0.44
2	100	1026	...	16	0.096	5	0.26
2	100	1026	0.5	16	0.096	5	0.26
2	100	1026	0.3	16	0.096	5	0.26
1	100	1026	0.3	21	0.079	12	0.16
2	50	1026	0.3	27	0.065	15	0.12
1	50	1026	0.3	34	0.055	16	0.097
1	20	1026	0.3	65	0.036	30	0.056

**Note.** The numbers listed in the sixth and eighth columns represent the uncertainty of the constraint on the dark energy equation of state. Results listed in the fifth and sixth (or seventh and eighth) columns are obtained by assuming that all the SMBBHs candidates have a mass ratio of  $q = 1$  (or  $q = 0.1$ ).  $N_s$  is the number of the sources that satisfy the condition of  $S/N > 10$  and  $\Delta d_L/d_L < 1.0$ . In the calculations, all SMBBH candidates are also assumed to have  $\iota = \pi/2$ . Note that in the first three cases no information from electromagnetic observations on the mass is added, so the fourth column is shown as a hyphen.

radius of the system, the GW frequency is  $f_{\text{GW}} = 2f_{\text{orb}}$ .<sup>6</sup> The green stars in Figure 1 mark the positions of those SMBBH candidates.

We consider a number of PTA settings on the number of usable MSPs ( $N_p$ ), pulsar timing noise rms  $\sigma_t$ , and the cadence  $\Delta t$ , which may be possible in the SKA era (as listed in Tables 1 and 2). With these PTA settings, the expected S/N for each SMBBH candidate can be calculated according to Equation (9). Figure 6 shows these SMBBH candidates in the  $M_{\text{tot}}-z$  plane and in the  $f_0-z$  plane, in which the objects with  $S/N > 10$  are marked with red circles. It is evident that only the SMBBH candidates with large  $M_{\bullet}$  (or correspondingly large chirp mass  $M_c$ ) are detectable in the SKA-PTA era (e.g., with  $S/N > 10$ ). However, the dependences on frequency  $f_0$  and redshift  $z$  are not significant. Figure 7 shows the expected S/N and the precision of luminosity distance measurements ( $\Delta d_L/d_L$ ) of those SMBBH candidates (assuming  $q = 1$ ) from PTAs with different settings. The determination of  $d_L$  is quite good for sources with large  $M_{\bullet}$  and high S/N (e.g.,  $> 10$ ). For these sources, if a mass ratio of  $q = 1$  is assumed, then there will be more sources that can have relatively accurate  $d_L$  measurements (with small  $\Delta d_L/d_L$ ); however, the number of such sources is substantially smaller if a smaller mass ratio is adopted ( $q = 0.1$ ; see Table 1) because of much weaker GW signals.

We only choose those sources with  $S/N \rho > 10$  and  $\Delta d_L/d_L < 1$  to estimate the precision of constraint on the dark energy EoS  $\Delta w$  that may be obtained from PTA observations. The reason is that only sources with sufficiently high S/N can be detected by PTAs and only sources with sufficiently small  $\Delta d_L/d_L$  are useful to obtain strong constraints on dark energy. If the sampling rate can be enhanced (smaller cadence  $\Delta t$ ; see Equation (9)), S/N approximately  $\propto N^{1/2} \propto 1/\sqrt{\Delta t}$  or the

<sup>6</sup> In principle, eccentric SMBBHs can be considered, though it is more complicated than circular ones as the GW emission is not monochromatic and an additional assumption needs to be made for the eccentricity distribution. We assume all SMBBHs are on circular orbits for simplicity.

**Table 2**

Expected PTAs Constraints on the Equation of State of Dark Energy from Mock SMBBHs

$\Delta t$ (week)	$\sigma_t$ (ns)	$N_p$	$\sigma \ln M_c^z$	$\rho > 10$		$\rho > 50$	
				$N_s$	$\Delta w$	$N_s$	$\Delta w$
2	100	200	...	45	0.32	9	0.45
2	100	500	...	121	0.18	28	0.26
2	100	1026	...	211	0.13	65	0.18
1	100	1026	...	362	0.090	113	0.13
2	50	1026	...	606	0.063	202	0.093
1	50	1026	...	1020	0.045	394	0.063
1	20	1026	...	3102	0.020	1578	0.025
2	100	1026	0.5	33848	0.026	957	0.12
2	100	1026	0.3	33848	0.017	957	0.085
1	100	1026	0.3	66707	0.0089	2183	0.043
2	50	1026	0.3	128574	0.0048	4891	0.021
1	50	1026	0.3	242352	0.0026	10356	0.011

**Note.** Legend similar to that for Table 1. Results listed in the fifth and sixth (or seventh and eighth) columns are obtained by adopting those mock SMBBHs with  $\rho > 10$  (or  $\rho > 50$ ) and  $\Delta d_L/d_L < 1$ . Note that in the first seven cases no information from electromagnetic observations on the mass is added, so the fourth column is shown as a hyphen.

timing noise rms can be suppressed (smaller  $\sigma_t$ ; see Equation (9)),  $S/N \propto 1/\sigma_t$ , the S/N and luminosity distance measurements can both be improved and thus a better constraint on the dark energy EoS can be obtained. Therefore, according to the results obtained above and those listed in Table 1, we conclude that only those SMBBHs with large chirp mass could be treated as standard sirens and can be used to get a strong constraint on the EoS of dark energy  $\Delta w \sim 0.04\text{--}0.06$  under the most optimistic conditions (see the last row in Table 1, which displays values estimated by using Equation (15) as described in Section 2).

## 5.2. Mock SMBBHs from a Simple Galaxy Merger Model

In this section, we generate a mock sample of SMBBHs according to a simple galaxy merger model since SMBBHs were generally formed via galaxy mergers. The main input quantities for this model are the cosmic merger rate of galaxies and the relationship between MBH mass and host galaxy properties, which can all be given by observations. We assume that the time delay between the merger of two galaxies and formation of a central SMBBHs is short ( $\sim 1$  Gyr) comparing with the cosmic time (e.g., for detailed dynamical merging processes see, e.g., Yu 2002; Y. Chen et al. 2019, in preparation), therefore it can be ignored. After the SMBBH enters into the PTA band, its orbital decay dominates by the GW radiation and thus the environmental effect can also be ignored. We further assume that SMBBHs are well circularized at frequencies  $\gtrsim 10^{-9}$  Hz and thus considerations of the eccentricities of SMBBHs are not needed in the following calculations. For the central SMBBH, the masses of its two components can be estimated according to the relationship between MBH mass and galaxy properties (Kormendy & Ho 2013), such as stellar mass.

The comoving number density of SMBBHs is controlled by the galaxy-galaxy merger rate density, the relationship between MBH mass and galaxy properties, and the residential time of SMBBHs at a different semimajor axis (and thus different GW frequencies under the GW decay). For SMBBHs at redshift  $z$

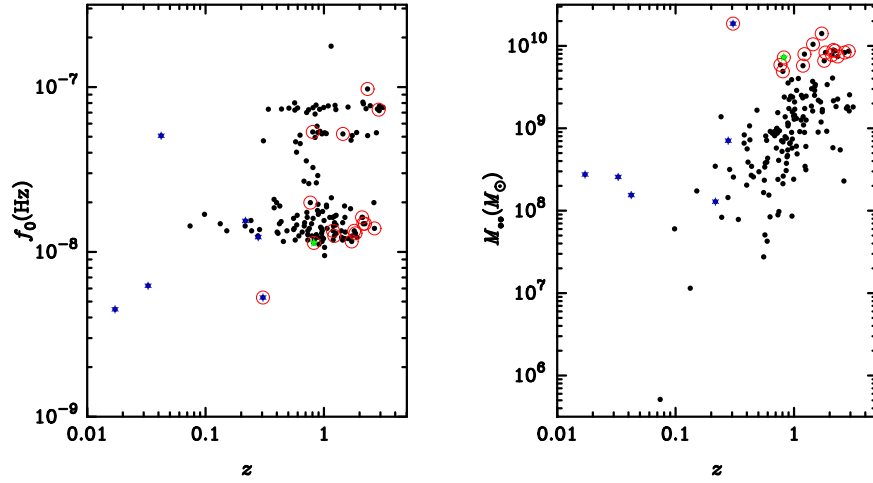


**Figure 6.** Distribution of SMBBH candidates (black points) in the  $f_0$ - $z$  plane (left) and in the  $M_*$ - $z$  plane (right). In each panel, the red circles mark those SMBBH candidates that their expected  $S/N > 10$  and  $\Delta d_L/d_L < 1.0$  if monitored by a PTA with  $N_p = 1026$ , a cadence of 2 weeks, and timing noise rms  $\sigma_t = 100$  ns. The SMBBH candidates are assumed to be of equal mass ( $q = 1$ ) and have  $\iota = \pi/2$ .

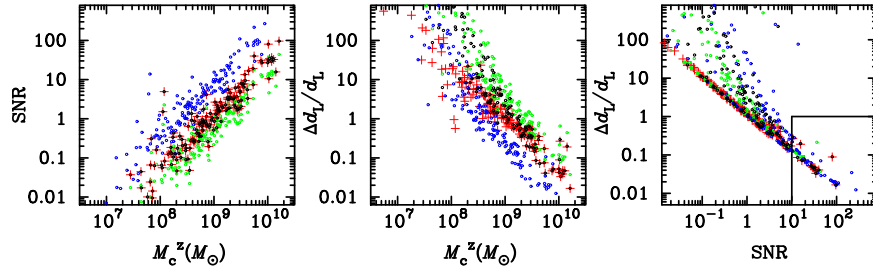


**Figure 7.** Expected signal-to-noise ratio (S/N) and luminosity distance measurement errors of those SMBBH candidates by a PTA with settings of  $(N_p, \iota, \sigma \ln M_c^2) = (1026, \pi/2, \dots)$  (black circles),  $(1026, \pi/2, 0.3)$  (red +),  $(200, \pi/2, \dots)$  (green circles), and  $(1026, \pi/10, \dots)$  (blue circles), respectively. Note that the results shown here are obtained by assuming  $q = 1$  for all SMBBH candidates.

with total mass  $M_*$  and mass ratio  $q$ , its comoving number density per unit comoving volume  $V$ ,  $q$ ,  $\log M_*$ , and logarithmic GW observed frequency  $\log f$  can be estimated as

$$\begin{aligned} \frac{dN(z, M_*, q, f)}{dV d \log f dq d \log M_*} &= \int d\mu_{\text{gal}} \int_0^\infty P(M_* | \bar{M}_*(M_{\text{gal}}, z)) \\ &\times \frac{dN_{\text{mrg}}}{d\mu_{\text{gal}} dt}(M_{\text{gal}}, \mu_{\text{gal}}, z) \delta(q - \mu_{\text{gal}}) \\ &\times \Phi(M_{\text{gal}}, z) \frac{\Delta t}{\Delta \log f} dM_{\text{gal}}. \end{aligned} \quad (16)$$

Here  $P(M_* | \bar{M}_*(M_{\text{gal}}, z))$  is assumed to be a Gaussian probability distribution function with a scatter of  $\Delta M_*$  that describes the distribution of the true MBH mass around the mean value  $\bar{M}_*(M_{\text{gal}}, z)$  obtained from the  $M_*$ - $M_{\text{bulge}}$  relationship given in Kormendy & Ho (2013), i.e.,  $\bar{M}_* = 0.49 \times 10^9 (M_{\text{gal}}/10^{11} M_\odot)^{1.17} M_\odot$  with a scatter of  $\Delta \log M_* = 0.3$ . The galaxy-galaxy merger rate  $\frac{dN_{\text{mrg}}}{d\mu_{\text{gal}} dt}(M_{\text{gal}}, \mu_{\text{gal}}, z)$  is obtained from the merger trees for galaxies in the Illustris Simulation by directly tracking the baryonic content of subhalos (Rodríguez-Gomez et al. 2015), where  $M_{\text{gal}}$  is the mass of the merger remnant galaxy,  $\mu_{\text{gal}}$  the mass ratio of the two progenitor galaxies.  $\Phi(M_{\text{gal}}, z)$  is the galaxy stellar-mass function, for which we adopt the estimates from Lopes et al. (2017, see Table 4 therein). Note that for

simplicity we assume  $q = \mu_{\text{gal}}$  and ignore the growth of MBHs before the formation of SMBBHs so that the total mass of the progenitor SMBBH equals the mass of MBH in the merger remnant galaxy. Since the orbital decay is governed by the GW radiation, the timeperiod  $\Delta t$  that an SMBBH stays at the frequency band from  $f$  to  $f + \Delta f$  is given by

$$\Delta t = \frac{8 \ln 10 (\pi f (1+z))^{-8/3}}{3 \frac{256}{5} (GM_c/c^3)^{5/3}} \Delta \log f. \quad (17)$$

We randomly generate mock SMBBHs in the parameter space of  $z \in (0, 4)$ ,  $f_0 \in (10^{-9} \text{ Hz}, 10^{-7} \text{ Hz})$ ,  $M_* \in (10^7 M_\odot, 10^{11} M_\odot)$ , and  $q \in (0.01, 1)$ , according to Equation (16) by integrating it over the cosmic volume. For each mock SMBBH, its sky location is randomly set by assuming a uniform distribution of SMBBHs on the two-dimensional sky. Its orbital inclination relative to the line of sight is randomly set over the range of  $\cos \iota \in [-1, 1]$ . We also fix the polarization angle  $\psi = 0$  and the initial phase angle  $\phi_0 = 0$ , for simplicity. With all the parameters set above, i.e.,  $(z, \alpha, \delta, \iota, M_*, q, f_0, \psi, \phi_0)$ , for each mock SMBBH, the S/N of its GW signal can be obtained for any given PTA. In the calculations of S/Ns, we assume that the sky position of those SMBBHs can be obtained by the EM signals from those SMBBHs, similar to the SMBBH candidates studied in Section 5.1.

We also consider a number of possible PTA settings in the SKA era as that in the previous Section 5.1 (see Tables 1 and 2). We adopt two different S/N thresholds for those mock

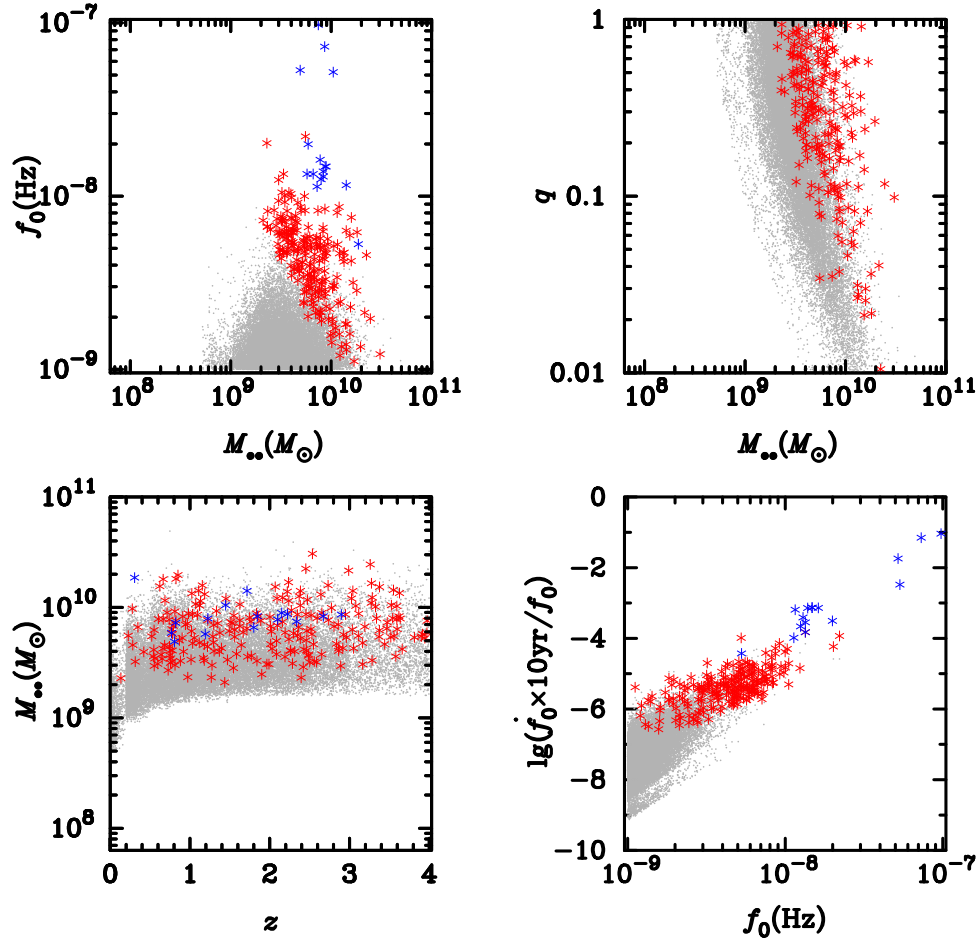


**Figure 8.** Distribution of SMBBHs in the  $f_0$  vs.  $M_{..}$  plane (top left),  $q$  vs.  $M_{..}$  plane (top right),  $M_{..}$  vs.  $z$  plane (bottom left), and  $\dot{f}_0/f_0$  vs.  $f_0$  plane (bottom right). In each panel, the gray dots show all mock SMBBHs in the simulated sample with  $S/N \rho > 10$ , red stars show the mock SMBBHs with  $\Delta d_L/d_L < 1$ , while blue stars (except in the top right panel) indicate those SMBBH candidates (assuming  $q = 1$ ) with  $\rho > 10$  and  $\Delta d_L/d_L < 1$ . The  $S/N$  for each mock SMBBH is estimated by assuming a PTAs observations with  $N_p = 1026$ , cadence  $\Delta t = 2$  weeks and  $\sigma_t = 100$  ns.

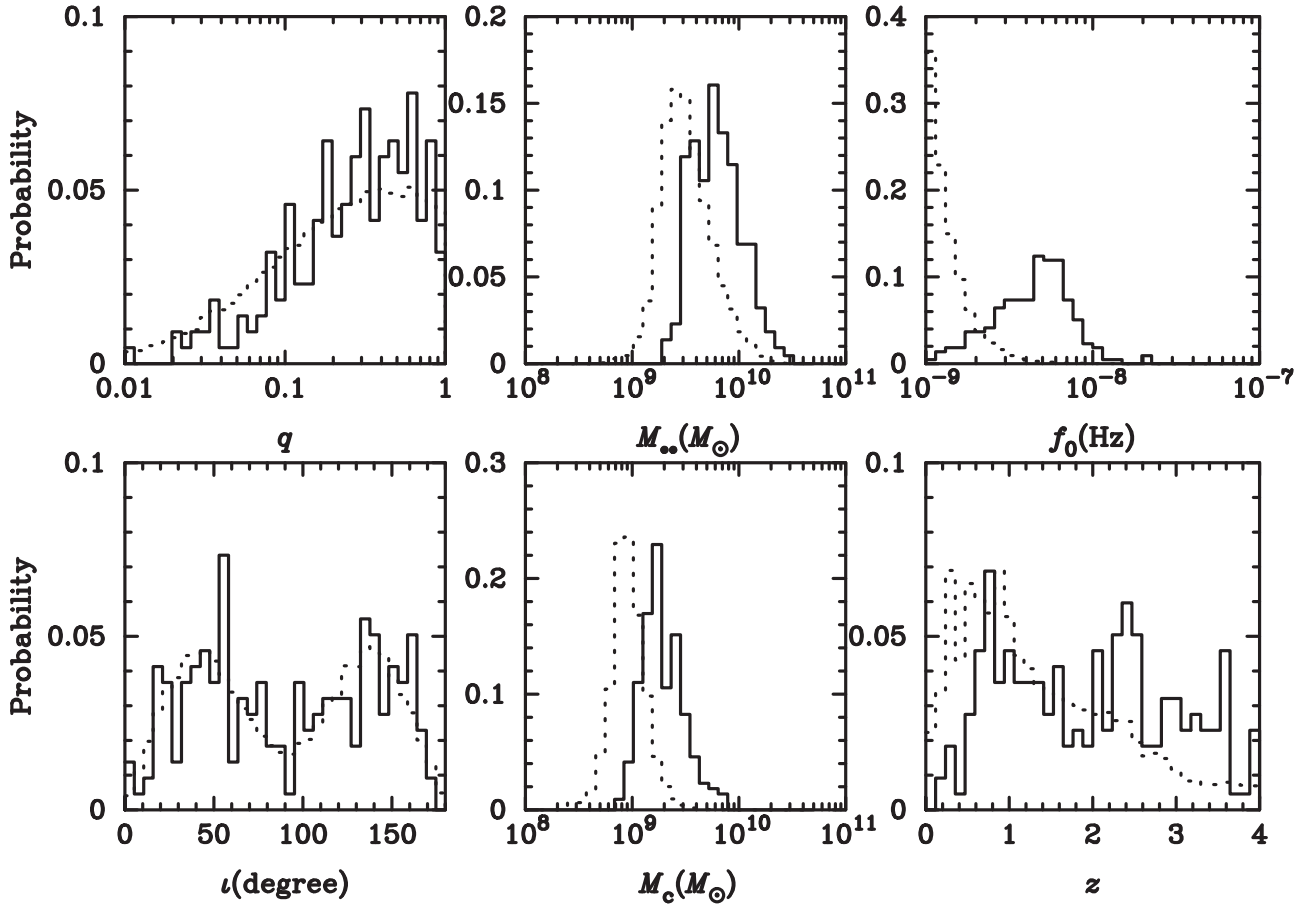
SMBBHs to be adopted in obtaining a constraint on the dark energy EOS, i.e.,  $\rho > 10$  and  $> 50$ , respectively. For the selected samples, using the Fisher matrix analysis, we derive the value of  $\Delta d_L/d_L$  and then obtain the constraint on the EoS of dark energy in different conditions as shown in Table 2. We illustrate our main results in Figures 8–10 as follows.

Figure 8 shows the distribution of both mock SMBBHs and observational SMBBH candidates (with  $\rho > 10$ ) on the plane of  $f_0$ – $M_{..}$  (top left panel),  $q$ – $M_{..}$  (top right panel),  $M_{..}$ – $z$  (bottom left panel), and  $\log(\dot{f}_0 \times 10 \text{ yr}/f_0)$ – $f_0$  (bottom right panel), respectively. The PTA adopted here has the settings of  $N_p = 1026$ ,  $\Delta t = 2$  weeks, and  $\sigma_t = 100$  ns, as shown by the third row in Table 2. Gray dots shown in this figure represent all the mock SMBBHs with  $S/N \rho > 10$ , while the red and blue stars mark the mock SMBBHs and observational SMBBH candidates with  $\rho > 10$  and  $\Delta d_L/d_L < 1$ . Only a small fraction of SMBBHs with  $\rho > 10$  that can have relatively good distance measurements  $\Delta d_L/d_L < 1$ , which can be used as the standard sirens.<sup>7</sup> The SMBBHs in this sample have relatively large  $M_{..}$

( $\gtrsim 3 \times 10^9 M_\odot$ , bottom left panel), relatively large  $f_0$  (top left panel), and relatively large  $\dot{f}_0/f_0$  (bottom right panel).

For comparison, Figure 9 shows the distributions of the total mass  $M_{..}$ , mass ratio ( $q$ ), chirp mass  $M_c$ , frequency  $f_0$ , inclination angle ( $\iota$ ), and redshift ( $z$ ) of SMBBHs in the selected SMBBH sample (red stars in Figure 8) and the whole sample (with  $\rho > 10$ , gray points in Figure 8). It is clear that the distributions of  $M_{..}$ ,  $f_0$ ,  $M_c$  in the selected sample are biased to the high-value ends from those in the parent SMBBH sample. The redshift distribution of SMBBHs in this selected sample is also different from that in the parent sample. The flat redshift distribution of SMBBHs in the selected sample suggests that usable PTAs SMBBH standard sirens can be detected at high redshift and thus offers a good tool to probe the high redshift universe. The distribution of  $\iota$  in the selected sample is more or less the same as that in the parent sample. The expected  $S/N$ s for SMBBHs with  $\iota \sim 90^\circ$  are relatively smaller, therefore, there is a lack of SMBBHs with such  $\iota$  in the selected sample (red stars). The lack of SMBBHs with  $\iota \sim 0^\circ$  or  $\sim 180^\circ$  are mainly caused by the random distribution of orbital orientation. The fraction of sources in the frequency range  $10^{-8}$ – $10^{-7}$  Hz is extremely small (top right panel of Figure 9) mainly because the higher frequency corresponds to the smaller SMBBH separation ( $a$ ) and thus much smaller residential time (as it proportional to  $a^4$ ). Most of the selected

<sup>7</sup> The four blue stars are quite faraway from the mock SMBBHs (top left panel and bottom right panel in Figure 8), which might be due to (1) some of the SMBBH candidates not being real SMBBHs, (2) the selection effects, or (3) our model underpredicting the abundance of SMBBHs at high frequency, though it is not likely.



**Figure 9.** Distributions of simulated SMBBHs against mass ratio  $q$  (top left), total mass  $M_*$  (top middle), initial frequency  $f_0$  (top right), polarization angle  $\iota$  (bottom left), chirp mass  $M_c$  (bottom middle), and redshift (bottom right). In each panel, the dotted histogram shows the distribution of all mock SMBBHs in the sample (with  $\rho > 10$ ), while the solid histogram shows that for those mock SMBBHs with  $S/N \rho > 10$  and  $\Delta d_L/d_L < 1$ .

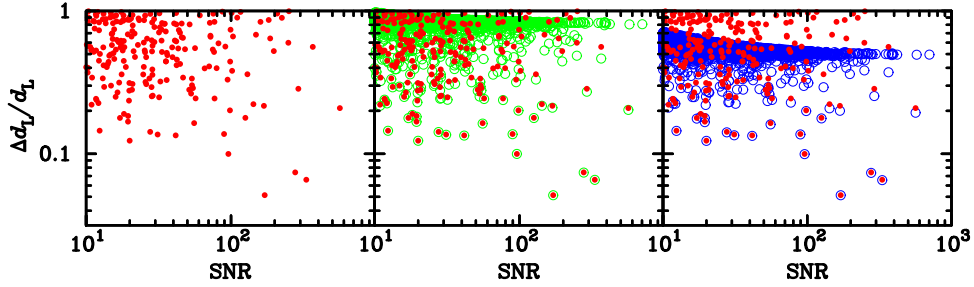


**Figure 10.** Expected errors of luminosity distance measurements for those mock SMBBHs (with  $\rho > 10$ ) by a PTA with pulsar number  $N_p = 1026$ , cadence  $\Delta t = 2$  weeks, and timing rms noise  $\sigma_t = 100$  ns. Left, middle, and right panels show the results obtained by assuming the chirp mass as a free parameter (red symbols), a free parameter with a  $1\sigma$  error of  $\sigma \ln M_c^z = 0.5$  (green circles), and 0.3 (blue circles), respectively. This figure shows that the measurements of luminosity distances from GW signals of many SMBBHs can be significantly improved if errors on chirp mass of SMBBH systems can be obtained from electromagnetic observations and thus the number of SMBBHs that can be used as standard sirens significantly increases with increasing precision of such additional information.

SMBBHs have  $f_0 < 10^{-8}$  Hz, where the frequency change rate is too small to be well measured by the PTAs and thus hinder the distance measurement with high precision.

If the SKA-PTA is conservatively set as  $\delta t = 2$  weeks and  $\sigma_t = 100$  ns, Using the mock SMBBHs with  $\rho > 10$  (or  $> 50$ ) and  $\Delta d_L/d_L < 1$  (red stars in Figure 8, only 211 with  $\rho > 10$  and 65 with  $\rho > 50$ ) as standard sirens, we can get an estimate of its constraining power on the dark energy for future PTAs (see the third row in Table 2). Apparently, the obtained constraint on the EoS of dark energy is about  $\Delta w \sim 0.1$ – $0.2$ , not very tight. If the SKA-PTA is optimistically set as  $\delta t = 1$  weeks and  $\sigma_t = 20$  ns, the mock SMBBHs with  $\rho > 10$  and

$> 50$  can be up to 3000 and 1500, respectively, with which the constraint on the EoS of dark energy can be achieved to the  $\sim 2\%$  level. For comparison, the potential constraints of EoS of dark energy by SN Ia or by weak lensing observations are expected to be around  $\Delta w \sim 0.01$  (Albrecht et al. 2006).

Electromagnetic observations of many PTA SMBBHs may enable the measurements of their physical properties, which may be combined with the PTA GW signal to improve the measurements of  $d_L$ . Such information includes the total mass and mass ratio of an SMBBH system, which can be obtained by the reverberation mapping technique and detailed analysis of its spectral energy distribution. Therefore, an estimation on the

error of the chirp mass is possible, which is not cosmological model dependent. Here we assume that the chirp mass accuracy can be obtained from electromagnetic observations to the order of  $\sigma \ln M_c^z \sim 0.5$  or  $0.3$  and consider the improvement of the constraints on the EoS of dark energy from the PTA SMBBHs. Figure 10 shows that the number of mock SMBBHs with  $\rho > 10$  and  $\Delta d_L/d_L < 1$  increases significantly if additional information on the chirp mass is put into the analysis (see Tables 1 and 2). For those sources with  $\Delta d_L/d_L \lesssim 0.2$ – $0.3$ , the improvements in  $\Delta d_L/d_L$  are negligible as further improvements require much more accurate mass measurements than the electromagnetic observations can give (see the middle and right panels of Figure 10). As seen from the last few rows in Tables 1 and 2, the constraints on the EoS of dark energy ( $\Delta w$ ) can reach to  $\lesssim 1\%$  level in the most optimistic cases (see last three rows in Table 2) if considering that the error of chirp mass estimates from electromagnetic observation can of SMBBHs can be as accurate as  $\sigma \ln M_c^z \sim 0.3$ – $0.5$ . Such a constraint is quite accurate even comparing with the next generation of large-scale structure surveys (Albrecht et al. 2006).

## 6. Conclusions and Discussions

Nano-hertz frequency GWs from individual SMBBHs are expected to be detected by PTAs in the near future. These “PTA detected” SMBBHs may also be used as standard sirens to probe cosmology. In this paper, we investigate whether such “PTA detected” SMBBHs can be used to obtain independent distance measurements and put strong constraints on the EoS of dark energy. To do this, we adopt the Fisher information matrix for parameter estimations to the expected GW signals from those currently available SMBBH candidates and a mock sample of SMBBHs produced from a simple galaxy merger model. We find that the luminosity distance measurements from the GW signals of some SMBBHs with high S/N can be relatively accurate ( $\Delta d_L/d_L \lesssim 0.3$ – $0.5$ ), especially when the information on the mass and mass ratio provided by electromagnetic observations are considered. Assuming that the redshifts of “PTA detected” SMBBHs can be obtained from electromagnetic observations, the number of those SMBBHs, typically with chirp mass in the range from  $10^9$  to  $10^{10} M_\odot$  and frequency in the range from  $10^{-8}$  to  $10^{-9}$  Hz, that can be used as standard sirens, is expected to be up to hundreds of thousands. The number of SMBBHs that is expected to be detected with  $S/N > 10$  and  $> 50$  by future SKA–PTA with conservative (or optimistic) settings are  $\sim 200$  (or  $\sim 3000$ ) and  $\sim 60$  (or  $\sim 1500$ ), respectively. Using these SMBBHs as standard sirens can put constraints on the EoS of dark energy to an uncertainty of  $\Delta w \sim 0.1$  (or  $\sim 0.02$ ). If the chirp mass for SMBBHs can be obtained by electromagnetic observations to a precision of  $\sigma \ln M_c \lesssim 0.5$  or higher, the number of “PTA detected” SMBBHs with  $S/N > 10$  and  $> 50$  can be  $\sim 30,000$ – $242,000$  and  $\sim 1000$ – $10,000$ , respectively, depending on different PTA settings. With these SMBBHs, the constraint on the EoS of dark energy can be  $\Delta w \lesssim 0.01$ – $0.1$ .

In our simple model to generate SMBBHs by major mergers of galaxies, the produced SMBBHs are assumed to have the same mass ratio as those of their merging progenitor galaxies. In reality, those SMBBHs may have a mass ratio different from their parent merging galaxies, partly due to the scatters in the  $M_*$ – $M_{\text{gal}}$  relation adopted to estimate black mass in individual galaxies and partly due to the growth of black holes during the merging processes. The former one may lead to more massive

black holes, and the latter one may cause the increase of the mass ratio and thus the chirp mass of SMBBHs because the secondary black holes may accrete more gas than the primary ones. Therefore, the number of SMBBHs that can be used as the standard sirens may increase significantly, and consequently lead to a better constraint on the EoS of dark energy presented above.

We also note that it is important to get accurate distance measurements in order to use the “PTA detected” SMBBHs as standard sirens. However, most “PTA detected” SMBBHs should have GW frequency  $\lesssim 10^{-8}$  Hz and negligible frequency change rates, which hinder accurate measurements of redshifted chirp mass and luminosity distance. On the one hand, if there are a number of SMBBHs (e.g., 100), like those among the SMBBH candidates (bottom left panel of Figure 8, with  $f_0 \sim 10^{-8}$ – $10^{-7}$  Hz) can have a significant frequency change rate, their chirp masses and distances may be well determined from the GW signals themselves, and thus lead to constraints on the EoS of dark energy with considerable precision (e.g.,  $\Delta w \lesssim 0.1$ ). On the other hand, if the total mass and mass ratio of SMBBHs, and thus the chirp mass, can be obtained from electromagnetic monitoring of those systems with high accuracy, then the luminosity distance measurements would be improved a lot. However, this requires dedicated studies for many individual “PTAs detected” SMBBHs.

We appreciate the helpful discussions with Xingjiang Zhu, Yan Wang, Linqing Wen, and Kejia Lee. This work is partly supported by the National Natural Science Foundation of China (grant Nos. 11690024, 11773028, 11603020, 11633001, 11173021, 11322324, 11653002, 11421303, and 11873056), the National Key Program for Science and Technology Research and Development (grant No. 2016YFA0400704), and the Strategic Priority Program of the Chinese Academy of Sciences (grant No. XDB 23040100).

## ORCID iDs

Changshuo Yan  <https://orcid.org/0000-0001-9736-1547>  
Youjun Lu  <https://orcid.org/0000-0002-1310-4664>

## References

- Abbott, B. P., Abbott, R., Abbott, T. D., et al. 2017a, *PhRvL*, **119**, 161101  
Abbott, B. P., Abbott, R., Abbott, T. D., et al. 2017b, *ApJL*, **848**, L12  
Abbott, B. P., Abbott, R., Abbott, T. D., et al. 2017c, *Natur*, **551**, 85  
Abbott, B. P., Abbott, R., Abbott, T. D., et al. 2019, *PhRvX*, **9**, 031040  
Aggarwal, K., Arzoumanian, Z., Baker, P. T., et al. 2019, *ApJ*, **880**, 116  
Albrecht, A., Amendola, L., Bernstein, G., et al. 2009, arXiv:0901.0721  
Albrecht, A., Bernstein, G., Cahn, R., et al. 2006, arXiv:astro-ph/0609591  
Arun, K. G., Mishra, C. K., Van Den Broeck, C., et al. 2009, *CQGra*, **26**, 094021  
Arzoumanian, Z., Baker, P. T., Brazier, A., et al. 2018a, *ApJ*, **859**, 47  
Arzoumanian, Z., Brazier, A., Burke-Spolaor, S., et al. 2014, *ApJ*, **794**, 141  
Arzoumanian, Z., Brazier, A., Burke-Spolaor, S., et al. 2016, *ApJ*, **821**, 13  
Arzoumanian, Z., Brazier, A., Burke-Spolaor, S., et al. 2018b, *ApJS*, **235**, 37  
Babak, S., & Sesana, A. 2012, *PhRvD*, **85**, 044034  
Charisi, M., Bartos, I., Haiman, Z., et al. 2016, *MNRAS*, **463**, 2145  
Chen, H.-Y., Fishbach, M., & Holz, D. E. 2018, *Natur*, **562**, 545  
Chernoff, D. F., & Finn, L. S. 1993, *ApJL*, **411**, L5  
Corbin, V., & Cornish, N. J. 2010, arXiv:1008.1782  
Desvignes, G., Caballero, R. N., Lentati, L., et al. 2016, *MNRAS*, **458**, 3341  
Ellis, J. A., Siemens, X., & Creighton, J. D. E. 2012, *ApJ*, **756**, 175  
Finn, L. S. 1996, *PhRvD*, **53**, 2878  
Finn, L. S., & Lommen, A. N. 2010, *ApJ*, **718**, 1400  
Graham, M. J., Djorgovski, S. G., Stern, D., et al. 2015a, *MNRAS*, **453**, 1562  
Graham, M. J., Djorgovski, S. G., Stern, D., et al. 2015b, *Natur*, **518**, 74  
Guo, H., Liu, X., Shen, Y., et al. 2019, *MNRAS*, **482**, 3288

- Hirata, C. M., Holz, D. Z., & Cutler, C. 2010, *PhRvD*, **81**, 124046
- Hotokezaka, K., Nakar, E., Gottlieb, O., et al. 2019, *NatAs*, **3**, 940
- Jaffe, A. H., & Backer, D. C. 2003, *ApJ*, **583**, 616
- Jenet, F. A., Hobbs, G. B., van Straten, W., et al. 2006, *ApJ*, **653**, 1571
- Kormendy, J., & Ho, L. C. 2013, *ARA&A*, **51**, 511
- Lee, K. J., Wex, N., Kramer, M., et al. 2011, *MNRAS*, **414**, 3251
- Lentati, L., & Shannon, R. M. 2015, *MNRAS*, **454**, 1058
- Lentati, L., Shannon, R. M., Coles, W. A., et al. 2016, *MNRAS*, **458**, 2161
- Li, Y.-R., Wang, J.-M., Ho, L. C., et al. 2016, *ApJ*, **822**, 4
- Li, Y.-R., Wang, J.-M., Zhang, Z.-X., et al. 2019, *ApJS*, **241**, 33
- Liu, X., Shen, Y., Bian, F., Loeb, A., & Tremaine, S. 2014, *ApJ*, **789**, 140
- Lopes, A. R., Gruppioni, C., Ribeiro, M. B., et al. 2017, *MNRAS*, **471**, 3098
- Madison, D. R., Zhu, X.-J., Hobbs, G., et al. 2016, *MNRAS*, **455**, 3662
- Maggiore, M. 2008, *Gravitational Waves, Vol. 1: Theory and Experiments* (Oxford: Oxford Univ. Press)
- Noysena, K., Klotz, A., Boër, M., et al. 2019, *ApJ*, **886**, 73
- Perera, B. B. P., DeCesar, M. E., Demorest, P. B., et al. 2019, *MNRAS*, **490**, 4666
- Perera, B. B. P., Stappers, B. W., Babak, S., et al. 2018, *MNRAS*, **478**, 218
- Planck Collaboration, Ade, P. A. R., Aghanim, N., et al. 2016, *A&A*, **594**, A13
- Planck Collaboration, Aghanim, N., Akrami, Y., et al. 2018, arXiv:1807.06209
- Rajagopal, M., & Romani, R. W. 1995, *ApJ*, **446**, 543
- Ravi, V., Wyithe, J. S. B., Shannon, R. M., et al. 2014, *MNRAS*, **442**, 56
- Ravi, V., Wyithe, J. S. B., Shannon, R. M., et al. 2015, *MNRAS*, **447**, 2772
- Reardon, D. J., Hobbs, G., Coles, W., et al. 2016, *MNRAS*, **455**, 1751
- Riess, A. G., Casertano, S., Yuan, W., et al. 2019, *ApJ*, **876**, 85
- Rodriguez-Gomez, V., Genel, S., Vogelsberger, M., et al. 2015, *MNRAS*, **449**, 49
- Rosado, P. A., Sesana, A., & Gair, J. 2015, *MNRAS*, **451**, 2417
- Schutz, B. F. 1986, *Natur*, **323**, 310
- Sesana, A. 2013, *MNRAS*, **433**, L1
- Sesana, A., Haiman, Z., Kocsis, B., et al. 2018, *ApJ*, **856**, 42
- Sesana, A., & Vecchio, A. 2010, *PhRvD*, **81**, 104008
- Sesana, A., Vecchio, A., & Volonteri, M. 2009, *MNRAS*, **394**, 2255
- Shannon, R. M., Ravi, V., Lentati, L. T., et al. 2015, *Sci*, **349**, 1522
- Shen, Y., Greene, J. E., Strauss, M. A., et al. 2008, *ApJ*, **680**, 169
- Smits, R., Kramer, M., Stappers, B., et al. 2009, *A&A*, **493**, 1161
- Thorne, K. S. 1987, in *Three Hundred Years of Gravitation*, ed. S. Hawking & W. Israel (Cambridge: Cambridge Univ. Press), 330
- Valtonen, M. J., Lehto, H. J., Nilsson, K., et al. 2008, *Natur*, **452**, 851
- Wahlquist, H. 1987, *GRGr*, **19**, 1101
- Wang, Y., & Mohanty, S. D. 2017, *PhRvL*, **118**, 151104
- Wang, Y., Mohanty, S. D., & Jenet, F. A. 2014, *ApJ*, **795**, 96
- Wyithe, J. S. B., & Loeb, A. 2003, *ApJ*, **590**, 691
- Yan, C.-S., Lu, Y., Dai, X., et al. 2015, *ApJ*, **809**, 117
- Yu, Q. 2002, *MNRAS*, **331**, 935
- Zhao, W., van den Broeck, C., Baskaran, D., & Wen, L. 2011, *PhRvD*, **83**, 023005
- Zhao, W., & Wen, L. 2018, *PhRvD*, **97**, 064031
- Zheng, Z.-Y., Butler, N. R., Shen, Y., et al. 2016, *ApJ*, **827**, 56
- Zhu, X.-J., Wen, L., Hobbs, G., et al. 2015, *MNRAS*, **449**, 1650